Applied Environmental Research
- RESEARCH FOR SUSTAINABLE PLANET -

Research Article

Spatiotemporal Patterns of Land Surface Temperature, Urban Heat Island, and Potential Heat Stress Risk Areas Assessment for Tropical Inland City and Coastal City in Thailand

Thar Htet Aung, Sakpod Tongleamnak*, Rasamee Suwanwerakamtorn

College of Computing, Khon Kaen University, Khon Kaen, 40002 Thailand

*Correspondence Email: sakpod@kku.ac.th

Abstract

Global warming and rapid urban growth, compounded by the urban heat island (UHI) effect, are posing substantial challenges for urban populations and ecological well-being due to increased heat stress risks. This study aimed to analyze the spatiotemporal patterns of land surface temperature (LST), UHI, and potential heat stress risk areas (PHSRA) in two distinct cities, an inland city, Nakhon Ratchasima, and a coastal city, Si Racha, during the summer. Geoinformatics techniques and Crichton's Risk Triangle method were employed, using updated demographic data and Sentinel-3 data from 2017 to 2022. The findings indicate that the inland city daytime average LST values were higher than in the coastal city, while the opposite was true at nighttime. Additionally, high daytime UHI patterns in the inland city were observed on the outskirts, and nighttime UHI concentrated in the urban center. The coastal city exhibited a strong daytime and nighttime UHI compared to the inland city, with daytime UHI peaking in the inner area and nighttime UHI near the coastline. The PHSRA was categorized into five risk levels (very high: > 0.8, high: 0.8–0.6, moderate: 0.6–0.4, low: 0.4–0.2 and very low: ≤ 0.2). During the daytime the highest risk areas, the high and very high levels of PHSRA in the inland city (23.84%) were greater than those in the coastal city (16.46%). Conversely, at nighttime, the coastal city (16.46%) exhibited higher levels than the inland city (5.26%). In nighttime conditions, all levels of PHSRA occurred more significantly than during the daytime in these cities. Understanding the spatiotemporal variations in PHSRA is vital for pinpointing places at risk of heat stress accidents in summer. This data is a goldmine for city planners and healthcare authorities, helping them plan interventions and effective measures for the future.

ARTICLE HISTORY
Received: 25 Dec. 2023
Accepted: 15 Aug. 2024
Published: 16 Sep. 2024

KEYWORDS
Spatiotemporal patterns;
Land surface temperature;
Urban heat island;
Heat stress risk;
Tropical city;
Thailand

Introduction

The world's population is rising dramatically, and while new cities are being developed, the current ones are becoming overcrowded [1]. Those changes in urbanization and urban land use will reach 1.2 million km^2, nearly tripling the global urban area in 2030 [2]. Rapid urbanization brings about significant changes in urban morphology and surfaces, along with a surge in anthropogenic heat emissions [3]. Heat islands develop due to the combined effect of these changes and raise air temperatures in urban regions more than in rural areas [4]. It is called UHI effect. This phenomenon and significantly worsens the quality of the outside air, resulting in heat-related illnesses and fatalities in metropolitan areas [5–6]. Due to the heightened air temperatures brought on by the higher population density and the UHI effect relative to their rural surroundings, extreme weather conditions particularly

https://doi.org/10.35762/AER.2024043

affect urban areas and can induce heat stress and other negative impacts [7–8]. High temperatures have also been identified as the primary contributor to weather-related fatalities [9]. Heat stress occurs when the human body cannot effectively dissipate metabolic heat, and the inner body temperature increases [10]. Ongoing urbanization, the combined impacts of climate change, and changes in demographics all work together to enhance the likelihood that city dwellers may experience heat-related stress [11–12]. Several research studies have highlighted the connection between UHI and increased mortality rates [13]. Nighttime UHI is generally more pronounced than daytime UHI. Nocturnal temperatures play a crucial role in human health, as elevated nighttime temperatures are associated with a heightened risk of heat-related mortality [14]. Commonly, when evaluating the risks associated with heat, the assessment encompasses not just heat-related hazards such as UHI or heatwaves, but also considers the vulnerability and exposure of the population [15].

UHI intensity is determined by using air temperature data from a weather station or the satellite data. LST is the Earth's surface temperature measured by its thermal radiation. Recent remote sensing advancements, like LST measurements [16–17], aid in UHI study. LST helps to create UHI indicators, including urban-suburban temperature differences and temperature distribution [18]. Both methods offer their distinct benefits. Although data on air temperatures is a direct indicator of UHI, it is only for specific sites. Since 2005, UHI studies have surged due to increased interest and better remote sensing [19]. In recent research endeavors, the application of remote sensing techniques has significantly enhanced our ability to gauge the spatial extent of the UHI at a finer resolution than previously achievable. Numerous investigations have leveraged satellite data to specifically address heat health risk assessments [20].

The UHI effect has reportedly been widely researched in cities and at locations throughout the globe, according to substantial literature for heat risk assessment. Different types of research have been conducted to investigate the link between LST and the composition and arrangement of man-made surfaces and green areas but they did not concentrate on social vulnerability [21–22]. Some heat risk studies pose a challenge in comprehending composite indices that amalgamate various indicator such as demographic, socio-economic, topographic, education, racial and language [23]. For instance, incorporated 25 indicators, while employed 9 variables to formulate a heat vulnerability index for Chicago and London [24–25]. This approach, however, constrains decision-makers in grasping the specific issues pertinent to the study areas, failing to elucidate why an area is susceptible. Moreover, prior investigations have often failed to delineate a specific vulnerable group, opting instead to amalgamate different vulnerable groups [15]. This method results in the suggested recommendations being overly broad or unsuitable for all vulnerable populations.

Furthermore, it is imperative to address a methodological concern related to the utilization of heat maps in heat risk assessments. Existing studies commonly rely on daytime and nighttime LST data from MODIS satellite observations, given the scarcity of Sentinel 3 satellite data. When conducting a comparative analysis between Sentinel 3 and MODIS, the research outcomes reveal a significant 90% overlap in pixel coverage. Nevertheless, a notable observation is the presence of a 10% commission error specifically in the MODIS dataset [26–27].

At present, a majority of research pertaining to the assessment of health risks associated with heat has predominantly taken place within developed nations. It is worth underscoring that the geographical dispersion of heat-related risks within developing countries remains relatively less understood [28]. Most of research has been predominantly concentrated on investigating heat-related risks within megacities [23, 25], while there have only been limited endeavors dedicated to scrutinizing these risks in medium-sized cities. Additionally, there remains a dearth of comparative analyses that have focused on the differences between the heat-related health risks for those living in inland urban areas versus coastal urban areas.

This study aims to compare the spatiotemporal distribution patterns of LST and UHI and Potential Heat Stress Risk Areas (PHSRA) in both the inland city of Nakhon Ratchasima and the coastal city of Si Racha during the summer season in Thailand. Both Nakhon Ratchasima and Si Racha were selected due to their distinct geographical and urbanization attributes. Nakhon Ratchasima exemplifies a medium-sized inland city situated on the northeast plateau of Thailand, showcasing typical characteristics of such areas. In contrast, Si Racha represents a medium-sized eastern coastal city, highlighting the coastal features of Thailand. The eastern coast is characterized by a diverse landscape, ranging from undulating and rolling hills to mountainous terrain, interspersed with flat lowlands that gently slope towards the sea. This diversity makes Si Racha an ideal case study for understanding coastal urban environments in Thailand. This investigation utilizes Sentinel-3 satellite data alongside updated demographic information. The methodology involves the creation of a spatially explicit map, emphasizing high-risk areas. The analysis delves into the constituent factors through the application of GIS and remote sensing techniques, incorporating

Crichton's Risk Triangle method. This research provides a scientific foundation for optimizing resource allocation and implementing effective intervention programs.

Materials and methods

1) Study area

The study areas are two distinct cities in Thailand (Figure 1). The inland city of Nakhon Ratchasima is situated in Nakhon Ratchasima Province at a considerable distance of approximately 275 kilometers away from the shores of the Gulf of Thailand. Its coordinates are 14° 58' 16'' N and 102° 5' 59'' E. The Lam Takong River flows from southwest to northeast through this area [29–30]. The city covers an area of 777.951 km^2 and is divided into 25 subdistrict municipalities, with a total population of 445,145 (572 people km^{-2}) in 2022.

The coastal city of Si Racha is located in Chonburi Province on the east coast of the Thailand. Its coordinates are 13° 10' 28'' N and 100° 55' 50'' E. In the study area, the north and northwestern parts feature mountainous regions and large water bodies, such as the Ban Bang Phra dam. On the west coast of the study area, there are small, isolated hills [31]. The district has 8 subdistricts, with a total land area of about 623.72 km^2 and with a resident population of over 338,898 (543 people km^{-2}) in 2022. Both the studied areas have a tropical savanna climate and tropical monsoon climate (Koppen climate classification Aw and Am). Typically, the summer season occurs from approximately mid-February to mid-May [32].

Nakhon Ratchasima, one of the most populous inland cities in northeastern Thailand, holds significant historical and economic importance. It was the terminus for Thailand's first railway line, connecting Bangkok to Nakhon Ratchasima. Additionally, the development of Mittraphap Road (Highway 2) further solidified the city's role as a crucial transportation and economic hub for the region [29–30]. On the other hand, Si Racha is renowned for its extensive industrial zone, encompassing manufacturing and shipping facilities. The city boasts the sprawling Laem Chabang Port, ranked as the 20th largest and busiest container port globally. Located in the southwestern part of the study area, this port plays a crucial role in Thailand's international trade and economic landscape [33]. In the past decades, the two cities have experienced unprecedented economic development and urban expansion, which has resulted in the intensified UHI effect and a large increase in heat-related health risks [34–35].

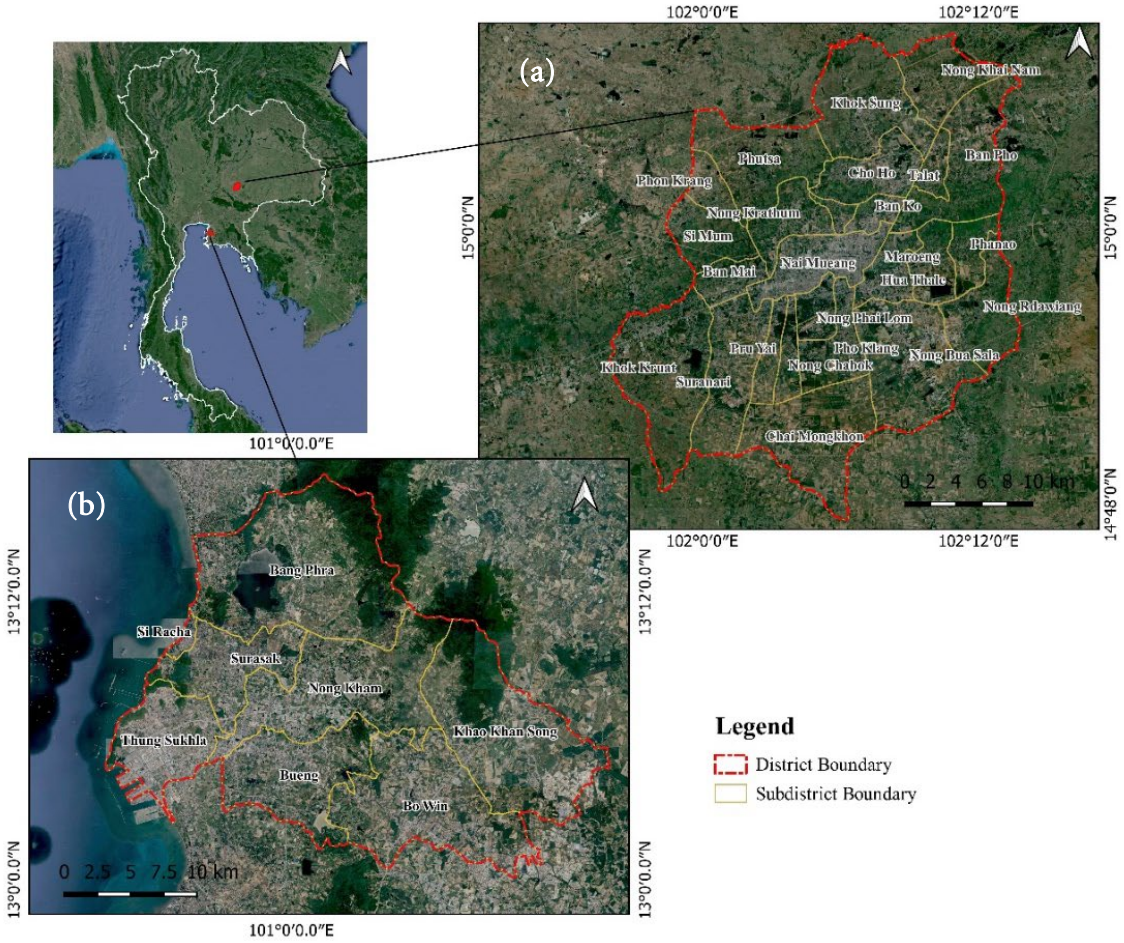

Figure 1 Location of two cities, (a) Nakhon Ratchasima and (b) Si Racha.

2) Data source

This study used daytime and nighttime Sentinel-3 LST. The studied areas aligned with Sentinel-3A and 3B paths, which pass over the region between 9:00-11:00 AM for daytime observations and 10:00 PM-12:00 AM (local time) for nighttime observations. However, these satellite overpass times may not coincide with the periods of peak UHI intensity or maximum LST. Consequently, the timing mismatch may result in underestimations of both UHI intensity and maximum LST values. A total of 48 cloud-free images were selected for short term this study, ranging from mid-February to mid-May of each year from 2017 to 2022. These images were chosen on a monthly basis, with two images captured during both daytime and nighttime for each month in the specified period. The e images used were acquired through the European Space Agency (ESA) Copernicus Open Access Hub for level 2, which were pre-processed in SNAP, while the geo-processing and the mapping of the results were developed in QGIS. All the data was re-projected (EPSG: 32647; WGS 84/UTM zone 47N) into the reference system.

Population density and the specific population are both important parameters for heat stress risk, and various studies have investigated their relationship with heat health risk. Population data information was collected from the official population statistics website of the Thai government, which was updated to 2022. The methodology involves collecting Sentinel 3 daytime and nighttime LST data and demographic data. Sentinel 3 LST values are converted from Kelvin to degrees Celsius, and daytime and nighttime UHI values are calculated for the study areas. These UHI (hazard parameter) values are then converted to vector data at the subdistrict level. Subdistrict level of population density (exposure parameter) and the percentage of the population under 5 years and over 65 years (vulnerability parameter) are calculated and included in the subdistrict-level vector data. The three parameters are normalized to a 0 to 1 scale and combined using a risk triangle method to identify potential heat stress risk areas at the subdistrict level. Finally, the integrated data undergo further normalization to classify different risk levels within the study areas. The employed research methodology is illustrated in Figure 2. It demonstrates the flow from data collection (Sentinel 3 and demographic data) through processing steps (conversion, calculation, normalization, and combination of parameters) to the final results (risk classification maps).

3) Crichton's risk triangle: PHSRA assessment framework

In this study, the development of the PHSRA index drew upon was based on Crichton's risk triangle approach, as outlined in previous works [32–34]. In this approach, Risk, characterized as the likelihood or potential for loss, was operationalized as a balanced amalgamation of exposure parameters, vulnerability parameters, and hazard parameters [38–39]. This approach is popular for three reasons: it's the simplest and most comprehensive way to assess risk; risk is seen as dynamic, influenced by three changeable components; and it's easy to break down into precise, transparent layers, making it suitable for the geospatial domain [40]. The concept of risk can be visualized through an imaginary equilateral triangle, where its three sides embody the three fundamental components of risk. The cumulative interplay of these components defines the overall risk, analogous to the area enclosed by the triangle. If any side is missing, there is no risk. Moreover, to lessen the risk, we must seek a better solution for all sides [36].

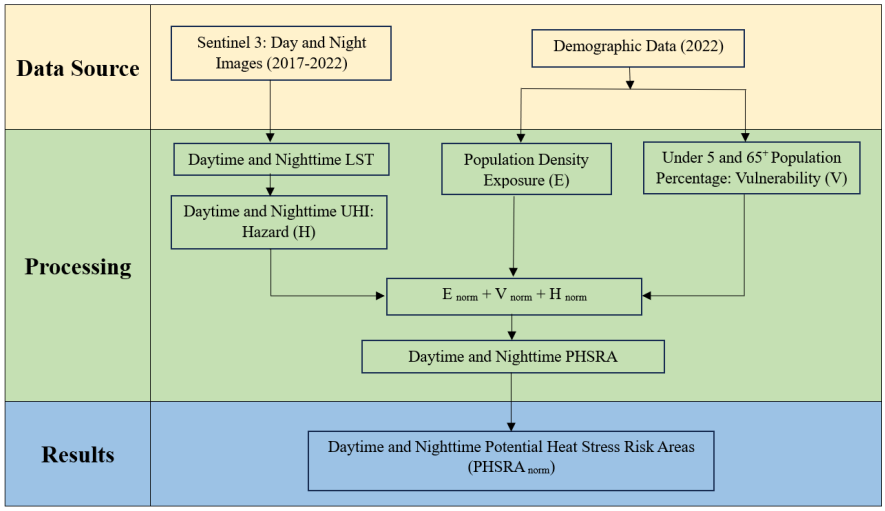

Figure 2 Research flow.

The three key parameters: exposure (E), vulnerability (V), and hazard (H) in this study are the following. Population density, measured in inhabitants per square kilometer, served as the exposure parameter (E). The vulnerability parameter (V) accounted for demographically sensitive groups, specifically the total population of young children (ages 0 to 5 years) and the elderly (ages 65 years and older) Urban Heat Island (UHI) intensity was utilized as the hazard parameter (H), following the approach outlined by Buscail C et al. [41].

Methods

1) Land surface temperature estimation

Focused on the idea of differential absorption by using the current SW algorithms to measure the LST, the difference between the two TIRS band wavelengths enables the signal to be adjusted for the effects of the atmosphere. TIRS band at two distinct wavelengths or a TIRS band at multiple opposite viewing angles can also be used for this. They are reliant on the emissivity of the earth's surface, which could be measured in a variety of methods [42]. Several papers have discussed the effectiveness, usefulness, and specificity of these algorithms in Sentinel 3 pictures [35, 42–47]. The official Sentinel 3 A and B level 2 SLSTR product's SW algorithm implicitly accounts for soil transmittance by using this Eq. 1 [48].

2) Urban heat island estimation

UHI is justified in the literature using contrasting temperatures observed simultaneously in the urban area and the rural areas around cities [49]. Remote sensing data is used to independently measure the surface heat island's intensity in urban and rural areas, and the selected pixels were examined in this context. Specified pixels and stations were the main sources of this evaluation, Eq. 2 [50–53].

3) Mapping of potential heat stress risk areas (PHSRA)

To quantify and map the PHSRA, key paramters including E, V and H were normalized from 0 to 1. Using the min-max method (Eq. 3), all variables were normalized on a 0 – 1 scale, in which 0 indicated a lower risk and 1 meant a higher risk. This was used for the normalization process [55].

After giving each factor a weight, these numbers were then merged into one index, the HERI. The characteristics were mixed especially by weighting E and V at 25% and H at 50% (Eq. 4), respectively.

$$LST = a_{f,i,pw} b_{f,i} (T_{11} - T_{12})^{\frac{1}{\cos\left(\frac{\theta}{m}\right)}} + (b_{f,i} + C_{f,i}) T_{12} - 237.15 \quad \text{(Eq. 1)}$$

where, the brightness temperatures of Sentinel 3 (bands 8 and 9) are represented by T_{11} and T_{12} are the brightness temperatures in the SLSTR 11 μm and 12 μm channels, while LST is represented by Kelvin. The values of a, b, and c are dependent on the type of plant cover and biome being observed. The variable θ represents the satellite's zenith angle of view, and while m is a dependent variable that is also affected by θ [35, 48].

$$UHI = \frac{(T_s - T_m)}{SD} \quad \text{(Eq. 2)}$$

where, T_s refers to the LST, T_m represents the mean of the LST, and SD for standard deviation [54].

$$Y_i = \frac{(x_i - \min(x))}{(\max(x) - \min(x))} \quad \text{(Eq. 3)}$$

in which, Y_i was defined as the normalized value of a dataset (E, V, H), which fell between 0 and 1. X_i could also be defined as the value of the dataset, in which min(X) represented the minimum value and max(X) represented the maximum value.

$$PHSRA = (0.25 \cdot E_{norm}) + (0.25 \cdot V_{norm}) + (0.50 \cdot H_{norm}) \quad \text{(Eq. 4)}$$

Eventually, using the max-min approach, the PHSRA was normalized (PHSRA norm) from 0 to 1 and mapping was done at the subdistrict level.

Based on the literatures [56-57], five risk levels were used to divide the HERI parameter for mapping as follows: very low (PHSRA≤0.2), low (0.2 < PHSRA ≤ 0.4), moderate (0.4 < PHSRA ≤ 0.6), high (0.6 < PHSRA ≤ 0.8) and very high (PHSRA > 0.8).

Results and discussion

1) Spatiotemporal distribution of LST

Table 1 present the statistics of the daytime and nighttime LST data for the two cities, obtained using the Sentinel 3 satellite images from 2017 to 2022. During the study period the average daytime LST for the inland city, Nakhon Ratchasima, was higher than that of the coastal city, Sri Racha. The average daytime LST for the inland city ranged from 34.25°C to 42.19°C, with a mean value of 39.10°C. In contrast, the coastal city's average daytime LST ranged from 28.30°C to 40.76°C, with a mean value of 34.31°C. During the nighttime, the coastal city exhibited higher average LST values, ranging from 24.44°C to 29.49°C, with a mean value of 26.45°C. In comparison, the inland city's average nighttime LST ranged from 24.23°C to 27.34°C, with a mean value of 25.93°C. Throughout the study period, daytime high average LST values of inland city was found outer and nighttime at city center. For coastal city, Sri Racha, daytime little far from coastal side and nighttime along the seaside (Figure 3 and Figure 4).

According to Table 1, the inland city, Nakhon Ratchasima, experienced its highest daytime mean LST value was recorded in 2020, reaching 40.57°C, while the lowest mean LST value occurred in 2021, at 37.87°C. At nighttime, the highest mean LST value was also observed in 2021, reaching 27.48°C, while the lowest mean LST value during was found in 2018, at 22.95°C. During the study period, the city center daytime LST values are consistently lower than the outer areas, with the most notable difference observed in the 2020 daytime LST distribution. Numerous studies attribute higher outer areas LST to increased long-wave radiation received due to building and tree shading in urban areas, along with cooling effects from urban green spaces. Conversely, during nighttime, the city center LST values are higher than the outer areas [58-59], particularly evident in the 2019 and 2021 nighttime LST distributions of the study area (Figure 3). These significant patterns were particularly evident during the years with the highest mean daytime and nighttime LST values of the inland city.

In the coastal city, the highest daytime mean LST value during the daytime occurred in 2019, with a value of 35.93°C, and the lowest mean LST value was recorded in 2018, at 32.24°C. Regarding the nighttime, the highest mean LST value was observed in 2020, reaching 26.91°C, while the lowest mean LST value was found in 2017, at 26.01°C. In Figure 4 illustrates that elevated daytime high LST values were observed to be slightly distant from the coastline, particularly in the inner north-western area. This pattern is notably evident in the daytime LST distribution for the years 2018 and 2022, which recorded the lowest mean LST values during the study period. Conversely, the higher nighttime LST values were identified predominantly along the coastline [60]. This pattern is especially pronounced in the 2022 nighttime LST distribution, which recorded the highest mean LST values of the entire study period.

Table 1 Daytime and nighttime LST (°C) in Nakhon Ratchasima and Si Racha during the summers from 2017 to 2022

Year	Nakhon Ratchasima (Inland city)								Si Racha (Coastal city)							
	Daytime LST (°C)				Nighttime LST (°C)				Daytime LST (°C)				Nighttime LST (°C)			
	Max	Mean	Min	SD	Max	Mean	Min	SD	Max	Mean	Min	SD	Max	Mean	Min	SD
2017	44.28	39.69	34.75	1.31	27.95	25.39	21.02	1.17	43.65	35.66	27.60	2.95	30.33	26.01	24.09	1.03
2018	41.48	38.34	33.89	1.25	26.94	24.95	22.26	0.90	39.31	32.24	26.70	2.10	29.86	26.12	23.82	0.92
2019	45.49	39.20	33.32	2.03	28.69	26.33	20.53	1.00	41.99	35.93	28.22	2.33	29.34	26.47	22.8	0.81
2020	45.33	40.57	35.37	1.78	27.52	25.61	23.17	0.52	41.42	33.85	27.24	2.27	29.85	26.91	23.75	0.80
2021	42.8	37.87	31.72	1.65	29.03	27.48	25.28	0.70	41.22	34.51	26.67	2.33	29.85	26.75	24.26	0.85
2022	42.01	38.17	32.51	1.70	27.91	25.65	23.74	0.66	39.82	33.23	26.39	2.56	29.45	26.5	22.49	0.84
Average	**42.19**	**39.10**	**34.25**	**1.22**	**27.34**	**25.93**	**24.23**	**0.59**	**40.76**	**34.31**	**28.30**	**1.98**	**29.49**	**26.45**	**24.44**	**0.78**

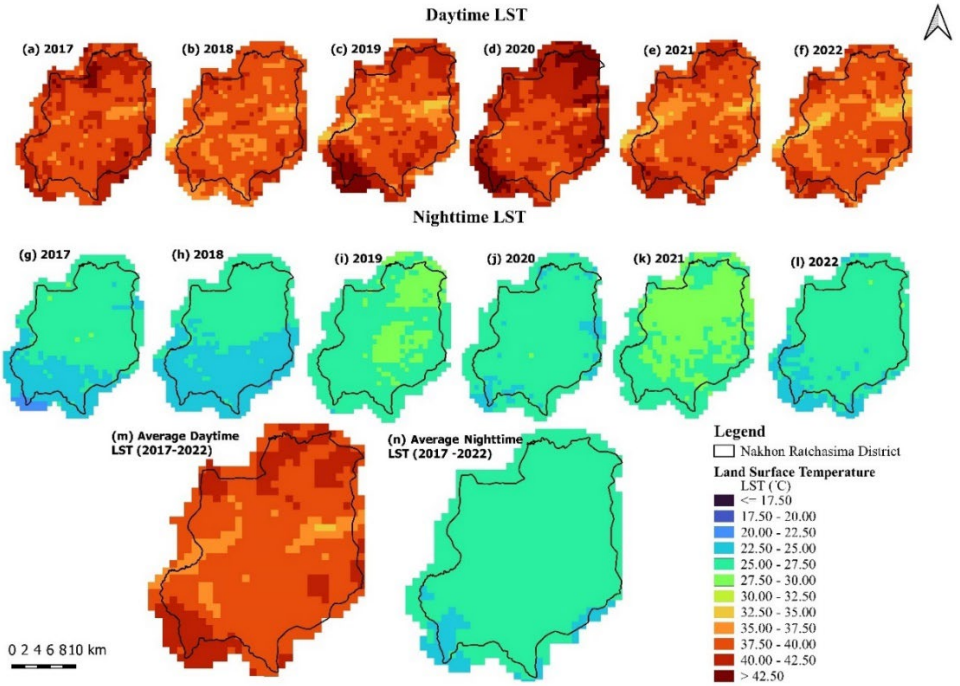

Figure 3 Daytime and nighttime LST distribution patterns of Nakhon Ratchasima during the summers from 2017 to 2022.

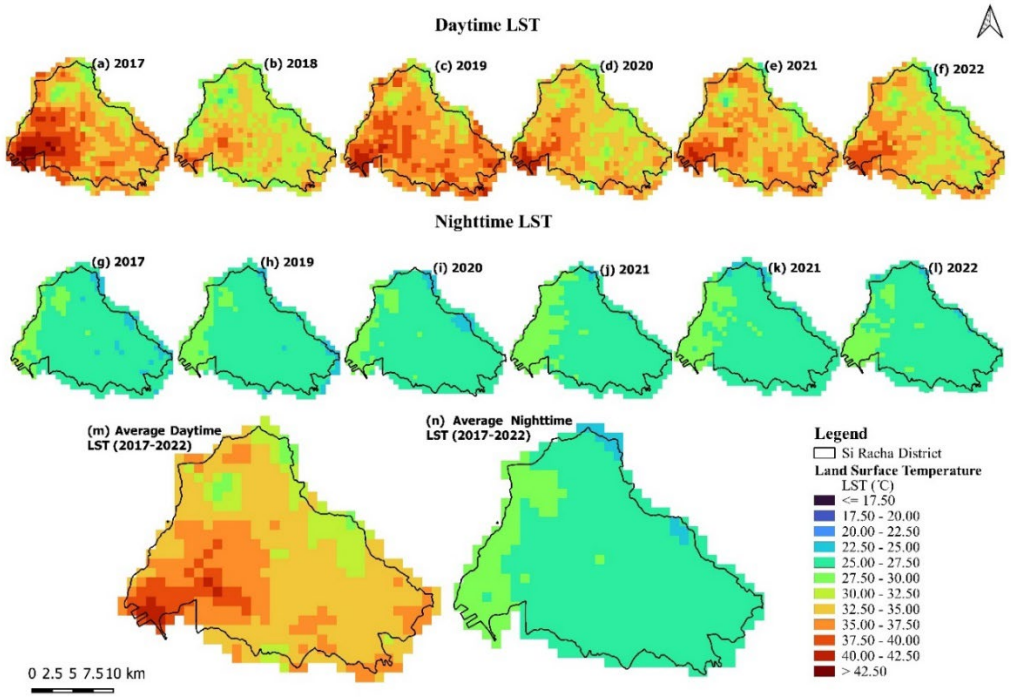

Figure 4 Daytime and nighttime LST distribution patterns of Si Racha during the summers from 2017 to 2022.

2) Spatiotemporal patterns of UHI

This study examined the UHI using Sentinel daytime and nighttime average LST data from 2017 to 2022 for both cities [57]. The coastal city, Sri Racha, exhibited higher average daytime and nighttime UHI values than the inland city, Nakhon Ratchasima. In the inland city, average daytime UHI values ranged from -3.96°C to 2.52°C with a mean value of 0.01°C, while nighttime values fluctuated between -2.87°C and 2.39°C with a mean of 0.02°C during study period. Conversely, for the coastal city, average daytime UHI values ranged from -3.16 to 3.40 °C, with a mean of 0.04 °C, and nighttime values varied between -2.87 °C and 3.71 °C, with a mean of 0.14°C (Table 2). Notably, in both cities, nighttime mean UHI values were higher than daytime mean UHI values.

According to Figure 5, daytime UHI patterns were prominent in the outer areas of the inland city, while nighttime UHI patterns were stronger in the city center. During the daytime, the outskirts of the inland city

exhibit significant UHI patterns, characterized by contour lines indicating UHI increases of 1°C to 2°C. Conversely, the city center shows weaker UHI effects, with contour lines near 0°C. The northeast and southwest areas along the Lam Takong River display the lowest UHI values, ranging from -3°C to -1°C. At nighttime, UHI patterns intensify in the city center, with contour lines showing higher values of 1°C to 2°C. UHI intensity slightly diminishes towards the city outskirts. Along the Lam Takong River, UHI values range from 0°C to 1°C. The lowest nighttime UHI values, ranging from -1°C to -2°C, are observed in the outer areas of the inland city.

In the coastal city, daytime UHI peaked slightly away from the coastline, while nighttime UHI patterns were high along the coastline and gradually decreased in an eastward direction within the study area. During the daytime, the southwestern part of the study area, particularly around Laem Chabang Port, exhibited the highest UHI intensity values, ranging from 1°C to 3°C, as depicted by contour lines. Conversely, areas along the eastern coast showed lower UHI intensity, ranging from 0°C to -1°C. The lowest daytime UHI values, ranging from -1°C to -3°C, were observed in regions encompassing water bodies and mountainous area. At nighttime, the highest UHI values, ranging from 1°C to 3°C, were concentrated along the seaside and near water bodies. Further inner area of coastal city, UHI intensity decreased, with contour lines indicating values between 0°C to 1°C. Some central areas exhibited UHI values from 0°C to -1°C during the nighttime. The lowest nighttime UHI values, ranging from -1°C to -3°C, were observed in mountainous areas.

Table 2 Average UHI patterns of Nakhon Ratchasima and Si Racha during the summers from 2017 to 2022

	Nakhon Ratchasima (Inland city)				Si Racha (Coastal city)			
	UHI (C)				UHI (C)			
	Max	Mean	Min	SD	Max	Mean	Min	SD
Daytime	2.53	0.01	-3.96	1.00	3.4	0.04	-3.16	1.07
Nighttime	2.39	0.02	-2.87	1.01	3.71	0.14	-2.87	1.07

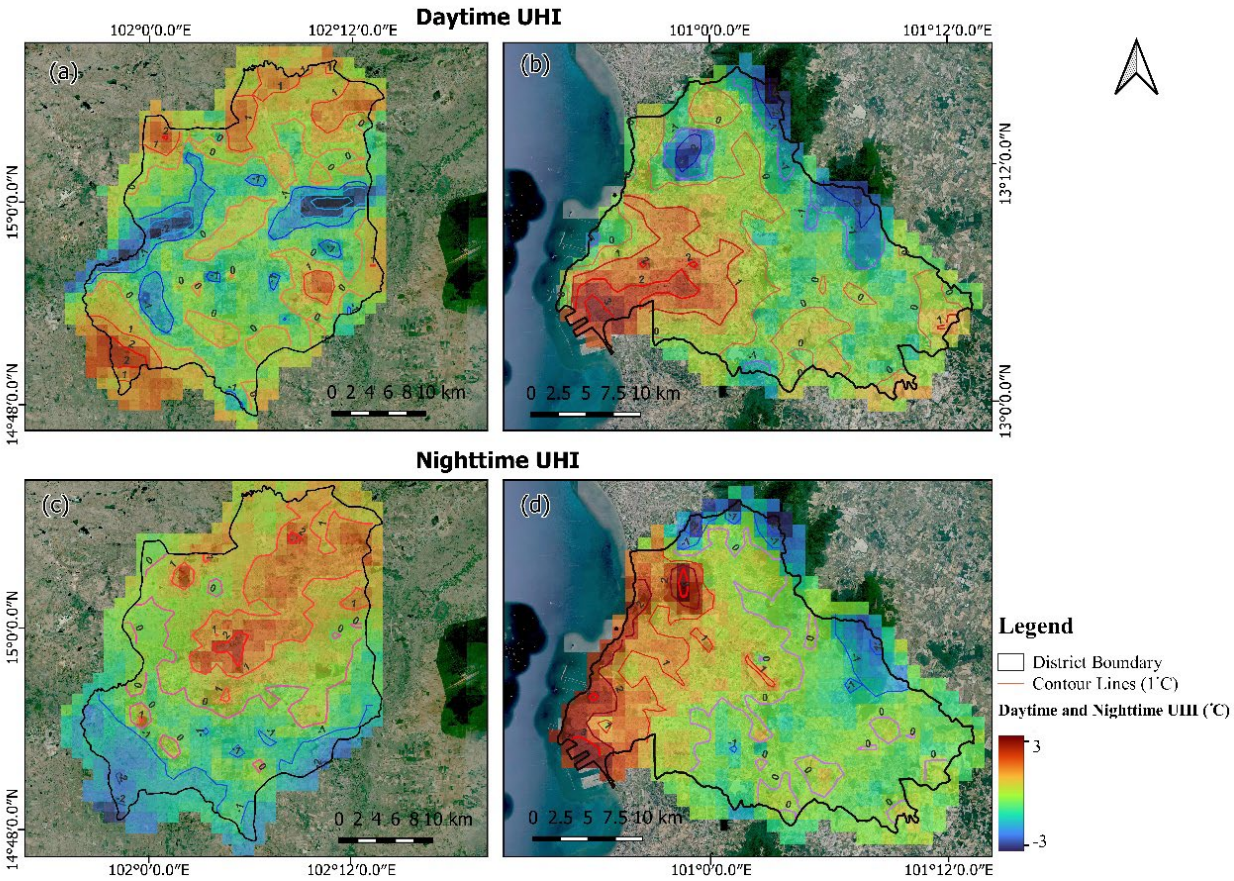

Figure 5 UHI patterns of Nakhon Ratchasima (a, c) and Si Racha (b, d) from 2017 to 2022.

3) Mapping of the PHSRA

Crichton's risk triangle evaluates the PHSRA for inland and coastal cities at the subdistrict level. The evaluation involved three parameters: population density (Exposure - E), the percentage of the population under 5 years and over 65 years (Vulnerability - V), and the UHI effect (Hazard - H). The same E and V parameters were used for both daytime and nighttime PHSRA calculations, while the H parameter was adjusted for daytime and nighttime UHI variations. In this calculation, population data from 2022 and average UHI values from 2017 to 2022 for both daytime and nighttime were used (Supplementary Material (SM) 1–13)).

3.1) Spatiotemporal PHSRA of the inland city

E parameter: Nai Mueang subdistrict had exhibited the highest population density with 3,265 inhabitants km^{-2}, followed by Muen Wai with 2,287 inhabitants km^{-2}. Conversely, the lowest population density had been recorded in the Chai Mongkhon subdistrict with 135 inhabitants km^{-2} (Table 3).

V parameter: Nai Mueang had emerged as the most vulnerable subdistrict, with 20.23% of its total population facing vulnerabilities. Phanao and Si Mum had been observed as the second-highest subdistricts, with 19.44% and 19.03% of their total populations facing vulnerabilities, respectively. Nonetheless, Ban Ko had had the lowest, with only 11.39% of its total population experiencing vulnerabilities.

Daytime H parameter: The highest daytime average UHI value had been observed in the Nong Khai Nam subdistrict at 0.90°C, followed by Khok Sung at 0.74°C. Interestingly, the lowest UHI value had been recorded in Phanao, where it had reached -1.66°C. During nighttime H parameter: Nai Mueang had exhibited the highest average UHI value at 1.50°C, while Ban Ko and Cho Ho had ranked second with 1.37°C and 1.25°C, respectively. Conversely, Khok Kruat had experienced the lowest average UHI value at -0.07°C throughout the study period.

According to the risk triangle method, Nai Mueang consistently exhibited the highest PHSRA during both daytime and nighttime, followed by Nong Khai Nan, Khok Sung, and Muen Wai subdistricts. In contrast, Maroeng shown the lowest PHSRA subdistrict. during the daytime, while Khok Kruat subdistrict found the lowest PHSRA during the nighttime. During the daytime, high to very high levels of PHSRA were found in 23.84% (185.45 km^2) of the total inland city area. Moderate level was found in 27.30% (212.36 km^2), and low to very low levels of PHSRA were found in 48.86% (380.14 km^2) of the total area. Transitioning to nighttime, the distribution shifted. About 5.26% (40.88 km^2) of the total area experienced high to very high PHSRA levels, whereas a larger portion, 37.82% (294.26 km^2), displayed a moderate level of PHSRA during the nighttime. Low and very low levels of PHSRA were found in 56.92% (442.82 km^2) of the total inland city area (Figure 6 (a, b)).

Table 3 Non-normalized values of E, V, H and PHSRA for Nakhon Ratchasima during the summers

No.	Subdistrict	Exposure (inh. /km^2)	Vulnerability (%)	Daytime hazard* (°C)	Nighttime hazard** (°C)	PHSRA (Day)	PHSRA (Night)
1	Cho Ho	577	15.12	-0.22	1.29	0.42	0.60
2	Si Mum	253	19.03	-1.10	-0.01	0.34	0.43
3	Muen Wai	2,287	16.87	-0.29	1.09	0.60	0.75
4	Khok Sung	197	17.83	0.74	0.88	0.66	0.57
5	Nai Mueang	3,265	20.23	0.01	1.50	0.83	0.99
6	Ban Pho	195	17.64	-0.06	1.11	0.49	0.61
7	Chai Mongkhon	135	15.49	-0.07	-0.77	0.43	0.17
8	Hua Thale	1,467	15.68	-0.82	0.72	0.39	0.58
9	Suranari	442	15.96	-0.24	-0.49	0.43	0.27
10	Nong Khai Nam	191	16.99	0.90	1.00	0.66	0.57
11	Phanao	338	19.44	-1.66	0.20	0.24	0.49
12	Nong Phai Lom	1,136	12.35	-0.48	1.05	0.34	0.52
13	Ban Ko	1,284	11.39	-0.09	1.37	0.40	0.57
14	Pru Yai	795	17.90	-0.13	-0.35	0.54	0.38
15	Khok Kruat	208	17.02	0.22	-1.07	0.53	0.16
16	Pho Klang	1,145	15.32	-0.43	-0.20	0.43	0.36
17	Talat	1,166	15.57	0.19	0.94	0.56	0.59
18	Phutsa	194	18.18	0.37	0.50	0.59	0.50
19	Maroeng	472	15.63	-1.48	0.52	0.18	0.46
20	Nong Rawiang	365	15.96	0.10	-0.59	0.49	0.24
21	Ban Mai	1,326	18.15	-1.26	0.22	0.36	0.54
22	Phon Krang	369	17.74	0.03	0.05	0.53	0.42
23	Nong Bua Sala	377	13.21	0.17	-0.52	0.43	0.18
24	Nong Chabok	1,295	17.47	-0.46	-0.17	0.50	0.44
25	Nong Krathum	413	14.62	-0.90	0.84	0.26	0.49

3.2) Spatiotemporal PHSRA of the coastal city

E parameter: Si Racha subdistrict had the highest population density, with 11,363 inhabitants km^{-2}. The second-highest population density had been observed in Surasak, with 1,446 inhabitants km^{-2}. Conversely, Khao Khangsong had recorded the lowest population density with 97 inhabitants km^{-2} (Table 4).

V parameter: Bang Phra subdistrict had had the highest vulnerability percentage at 18.94%, while Khao Khangsong and Si Racha followed closely with vulnerability percentages of 16.23% and 16.03% of their total populations, respectively. Bowin was found to have had the lowest vulnerability percentage 11.45% of its total population.

Daytime H parameter: Thung Sukla subdistrict had exhibited the highest average UHI value with 1.58°C, which was followed by Surasak and Bueng, which had been recorded at 0.77°C and 0.67°C, respectively. Conversely, Khao Khangsong showed the lowest daytime average UHI value at -0.52°C. During nighttime H parameter: Si Racha subdistrict had exhibited the highest average UHI value at 2.11°C, followed by Thung Sukla at 2.06°C. Khao Khangsong had shown the lowest nighttime average UHI intensity, measured at -0.59°C in the study area.

According to the risk triangle method, the highest PHSRA during both daytime and nighttime in the coastal city were found in Si Racah, followed by Thung Sukla and Surasak subdistricts. Bowin was identified with the lowest PHSRA subdistrict during both daytime and nighttime. During the day, high and very high levels of PHSRA covered 16.46% (102.72 km^2), while a moderately high level of PHSRA was found in 10.62% (66.23 km^2). Conversely, low and very low levels of PHSRA encompassed a larger portion at 72.91% (454.78 km^2) of the total coastal city area. At nighttime, high and very high levels of PHSRA covered the same area as during the day, and a moderately high level of PHSRA was found in 23.53% (146.69 km^2) of the total area. This constituted 60.01% (374.31 km^2), characterized by low and very low levels of PHSRA during nighttime (Figure 6 (c, d)).

3.3) Comparing to spatiotemporal PHSRA of the inland and coastal cities

Urban regions experiencing elevated heat risk levels did not consistently exhibit the highest temperatures [56]. Both inland and coastal city, areas with elevated heat risk levels also exhibit the highest concentrations of both total and vulnerability population densities [56–57]. Consequently, it is imperative to promptly administer healthcare services within these zones during instances of extreme heat events. During the daytime of inland city, high and very high levels of PHSRA are primarily located in the city center subdistricts, while they are mostly found in the outer subdistricts. However, at nighttime, the high and very high levels of PHSRA shift, with the city center subdistricts being predominantly affected and the risk slightly decreasing in the outer subdistricts. Consistent with previous research, the impact of heat was particularly noticeable among individuals residing in urban center neighborhoods [37, 40]. This phenomenon is attributed to the cumulative influence of UHI. During both daytime and nighttime, the coastal city was identified as having high and very high levels of PHSRA. These are primarily located in the seaside subdistricts, and the risk slightly decreases in the inner subdistricts, a situation that becomes particularly significant at nighttime. Daytime high and very high levels of PHSRA of inland city (23.84%) was higher than the coastal city (16.46%) and conversely at nighttime, coastal city (16.46%) was higher than inland city (5.26%). Daytime and nighttime, moderate level of PHSRA of inland city (27.30%, 37.82%) higher than coastal city (10.62%, 23.53%). Low and very low levels of PHSRA of coastal city (72.91%, 60.01%) higher than inland city (48.86%, 56.92%) at daytime and nighttime.

Table 4. Non-normalized values of E, V, H and PHSRA for Si Racha during the summers

No.	Subdistrict	Exposure (inh. /km^2)	Vulnerability (%)	Daytime hazard* (°C)	Nighttime hazard** (°C)	PHSRA (Day)	PHSRA (Night)
1	Si Racha	11363	16.03	0.17	2.11	0.57	0.90
2	Surasak	1446	15.45	0.77	1.70	0.47	0.59
3	Thung Sukla	835	13.68	1.58	2.06	0.59	0.58
4	Bueng	762	12.54	0.67	-0.10	0.33	0.14
5	Nong Kham	506	14.43	0.14	0.17	0.27	0.25
6	Khao Khangsong	97	16.23	-0.52	-0.59	0.16	0.16
7	Bang Phra	212	18.94	-0.51	0.33	0.25	0.42
8	Bowin	459	11.45	-0.07	-0.16	0.12	0.09

Note: *Daytime average UHI, ** Nighttime average UHI

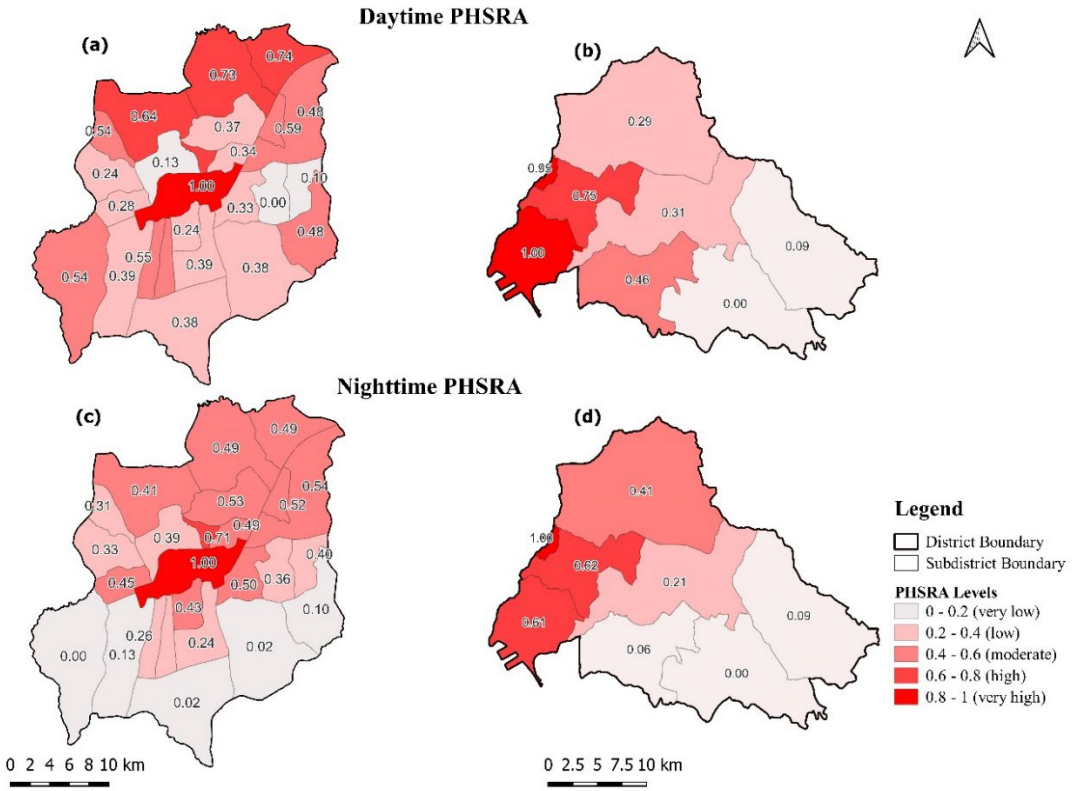

Figure 6 PHSRA maps of Nakhon Ratchasima (a, b) and Si Racha (c, d) during the summers of 2017–2022 (normalized values from 0 to 1).

Conclusion and discussion

The present research delved into an examination of the spatiotemporal variations in the LST and UHI patterns within inland and coastal cities, using of Sentinel 3 satellite images from 2017 to 2022. Subsequently, it employed the risk triangle methodology to explore the PHSRA mapping of the two cities during the summer.

Firstly, examining the LST patterns between the inland and coastal cities reveals distinct thermal dynamics. During the summer seasons from 2017 to 2022, the daytime average LST in the inland city consistently surpassed that of the coastal city, with average mean values of 39.10°C and 34.31°C, respectively. Conversely, during nighttime, the coastal city exhibited higher average LST values compared to the inland city, with mean values of 26.45°C and 25.93°C, respectively. These temperature differentials highlight the moderating influence of the coast on nighttime temperatures, leading to more stable patterns in the coastal city. Throughout the study period, the mean LST trends indicate that during the daytime and nighttime, there is no significant increase or decrease observed in either of cities.

Secondly, the analysis of UHI distribution patterns elucidates further disparities between the two cities. Despite modest mean UHI values close to zero in both cities during the study period, coastal city consistently exhibited slightly higher average UHI values (with mean values of 0.04 in daytime and 0.14 in nighttime) compared to inland city (with average mean values of 0.01 in daytime and 0.02 in nighttime). Notably, the spatial distribution of UHI showed intriguing patterns. In inland city, daytime UHI was more pronounced in outer areas, while nighttime UHI peaked in the city center. Conversely, coastal city displayed a different pattern with daytime UHI peaking slightly inland and nighttime UHI intensifying along the coastline. These findings highlight the significant influence of geography and environment on urban heat dynamics.

Thirdly, comparing the PHSRA between the two cities offers valuable insights into health vulnerability. Despite variations in UHI effects, areas with elevated PHSRA levels were consistently associated with high population density and vulnerability. In both cities, urban center subdistricts exhibited the highest PHSRA levels, particularly during nighttime, attributed to the cumulative influence of UHI. Examining the numerical breakdown of PHSRA levels further elucidates these disparities. In the daytime, high and very high levels of PHSRA areas were more prevalent in the inland city (23.84%) compared to the coastal city areas (16.46%), reflecting the intensified heat stress in urban centers. Conversely, at nighttime, the coastal city surpassed the inland city in high and very high PHSRA levels areas (16.46% vs. 5.26%), highlighting the exacerbation of heat stress along the coastline. Moderate PHSRA level areas were consistently higher in the inland city during

both daytime and nighttime, indicative of widespread heat vulnerability. Conversely, low and very low PHSRA levels areas were more prevalent in the coastal city, underscoring the mitigating effect of coastal proximity on heat stress risk. In conclusion, the spatiotemporal analysis of LST, UHI, and PHSRA patterns unveils the intricate relationship between urbanization, geographical location, and health vulnerability. Both cities face significant health risks associated with heat stress, particularly in densely populated urban centers. Understanding these dynamics is crucial for informing targeted interventions and urban planning strategies to mitigate the adverse effects of heat on public health and well-being.

The study has limitations as it solely used readily available secondary data from public sources. It's advised to regularly update PHSRA maps with the latest remote sensing and census data annually. Furthermore, examining how machine learning predictive models perform under different seasons can offer valuable insights. Comparing the effects of various urban parameters on both land surface temperature and air temperature is essential for a nuanced understanding. Moreover, the performance of urban vertical parameters, including building walls, street canyons, and roof types, warrants further investigation. Studying the variation of physiologically equivalent temperature (PET) within different heat risk categories and its response to land surface temperature and air temperature will provide insights into human comfort and health risks. Urban planners should take these findings into account when designing and implementing green spaces in urban areas, especially during the summer months. By incorporating these recommendations, future research can contribute significantly to mitigating heat stress risks in urban environments.

References

[1] Jansson, E. Reaching for a sustainable, resilient urban future using the lens of ecosystem services. Ecological Economics 2013, 86, 285–291.

[2] Seto, K.C., Guneralp, B., Hutyra, L.R. Global forecasts of urban expansion to 2030 and direct impacts on biodiversity and carbon pools. Proceedings of the National Academy of Sciences USA, 2012, 109, 16083–16088.

[3] Bernard, J., Musy, M., Calmet, I., Bocher, E., Keravec, P. Urban heat island temporal and spatial variations: Empirical modeling from geographical and meteorological data. Building and Environment, 2017, 125, 423–438.

[4] Santamouris, M. Analyzing the heat island magnitude and characteristics in one hundred Asian and Australian cities and regions. Science of the Total Environment, 2015, 512–513, 582–598.

[5] Basu, R., Samet, J.M. Relation between elevated ambient temperature and mortality: A review of the epidemiologic evidence. Epidemiologic Reviews, 2002, 24, 190–202.

[6] Doyon, B., Belanger, D., Gosselin, P. The potential impact of climate change on annual and seasonal mortality for three cities in Quebec, Canada. International Journal of Health Geographics, 2008, 7.

[7] Gabriel, K.M.A., Endlicher, W.R. Urban and rural mortality rates during heat waves in Berlin and Brandenburg, Germany. Environmental Pollution, 2011, 159, 2044–2050.

[8] Romero-Lankao, P., Qin, H., Dickinson, K. Urban vulnerability to temperature-related hazards: A meta-analysis and meta-knowledge approach. Global Environmental Change, 2012, 22, 670–683.

[9] Basu, R. Environmental Health High ambient temperature and mortality: A review of epidemiologic studies from 2001 to 2008.j Environmental Health, 2009, 8, 40.

[10] Gosling SN, Bryce EK, Grady Dixon P, A Gabriel KM, Gosling EY, Hanes JM, et al. A glossary for biometeorology, 2014, 58, 277–308.

[11] Lauf, S., Haase, D., Kleinschmit, B. Land-use scenario modelling based on human decisions – Combining system dynamics and cellular automata. International Environmental Modelling and Software Society, 2012, 12.

[12] Lauf, S., Haase, D., Hostert, P., Lakes, T., Kleinschmit, B. Uncovering land-use dynamics driven by human decision-making - A combined model approach using cellular automata and system dynamics. Environmental Modelling and Software, 2012, 27–28, 71–82.

[13] Hondula, D.M., Davis, R.E., Leisten, M.J., Saha, M.V., Veazey, L.M., Wegner, C.R. Fine-scale spatial variability of heat-related mortality in Philadelphia County, USA, from 1983-2008: A case-series analysis. Environmental Health, 2012, 11, 1–11.

[14] Kovats, R.S., Hajat, S. Heat stress and public health: A critical review. Annual Review of Public Health, 2008, 29, 41–55.

[15] Estoque, R.C., Ooba, M., Seposo, X.T., Togawa, T., Hijioka, Y., Takahashi, K., Nakamura, S. Heat health risk assessment in Philippine cities using remotely sensed data and social-ecological indicators. Nature Communications, 2020, 11, 1581.

[16] Sobrino, J.A., Caselles, V., Becker, F. Significance of the remotely sensed thermal infrared measure-

ments obtained over a citrus orchard. ISPRS Journal of Photogrammetry and Remote Sensing, 1990, 44, 343–54.

[17] Voogt, J.A., Oke, T.R. Thermal remote sensing of urban climates. Remote Sensing of Environment, 2003, 86, 370–384.

[18] Schwarz, N., Schlink, U., Franck, U., Großmann K. Relationship of land surface and air temperatures and its implications for quantifying urban heat island indicators - An application for the city of Leipzig (Germany). Ecological Indicators, 2012, 18, 693–704.

[19] Zhoua, W., Troya, A., Grove, M. A comparison of object-based with pixel-based land cover change detection in the Baltimore metropolitan area using multitemporal high resolution remote sensing data. International Geoscience and Remote Sensing Symposium (IGARSS), 2008, 4.

[20] Hendryx, M., Conley, J., Fedorko, E., Luo, J., Armistead, M. Permitted water pollution discharges and population cancer and non-cancer mortality: Toxicity weights and upstream discharge effects in US rural-urban areas. International Journal of Health Geographics, 2012, 11.

[21] Liou, Y.A., Nguyen, K.A., Ho, L.T. Altering urban greenspace patterns and heat stress risk in Hanoi city during Master Plan 2030 implementation. Land Use Policy, 202, 1, 105.

[22] Janicke, B., Holtmann, A., Kim, K.R., Kang, M., Fehrenbach, U., Scherer, D. Quantification and evaluation of intra-urban heat-stress variability in Seoul, Korea. International Journal of Biometeorology, 2019, 63, 1–12.

[23] Dugord, P.A., Lauf, S., Schuster, C., Kleinschmit B. Land use patterns, temperature distribution, and potential heat stress risk - The case study Berlin, Germany. Computers, Environment and Urban Systems, 2014, 48, 86–98.

[24] Johnson, D.P., Stanforth, A., Lulla, V., Luber, G. Developing an applied extreme heat vulnerability index utilizing socioeconomic and environmental data 2012.

[25] Wolf, T., Mcgregor, G. The development of a heat wave vulnerability index for London, United Kingdom, 2013.

[26] Freeborn, P.H., Wooster, M.J., Roberts, G., Malamud, B.D., Xu, W. Development of a virtual active fire product for Africa through a synthesis of geostationary and polar orbiting satellite data. Remote Sensing of Environment, 2009, 113, 1700–1711.

[27] Xu, W., Wooster, M., He, J., Environment TZ-RS of, 2020 undefined. First study of Sentinel-3 SLSTR active fire detection and FRP retrieval: Night-time algorithm enhancements and global intercomparison to MODIS and VIIRS AF. Elsevier, 2020, 248.

[28] Romero-Lankao, P., Qin, H., Dickinson, K. Urban vulnerability to temperature-related hazards: A meta-analysis and meta-knowledge approach. Global Environmental Change, 2012, 22, 670–683.

[29] Thebpanya, P., Bhuyan, I. Urban sprawl and the loss of peri-urban land: A case study of Nakhon Ratchasima Province, Thailand. Applied Geography, 2015, 1, 43–49.

[30] Seemuangngam, A., Lin, H.L. The impact of urbanization on urban flood risk of Nakhon Ratchasima, Thailand. Applied Geography, 2024, 162.

[31] Tatyaqupt, M., Charusiri, P., Ponsapich, W. Geology and stratigraphy of the Sri Racha area, Chonburi Province, Eastern Thailand. Bulletin of the Geological Society of Malaysia, 1986, 20, 59–71.

[32] Keeratikasikorn, C., Bonafoni, S. Urban heat island analysis over the land use zoning plan of Bangkok by means of Landsat 8 imagery. Remote Sensing, 2018, 10.

[33] Pleerux, N., Nardkulpat, A. identification of road accident recurrence in Sri Racha District, Chon Buri Province, 2019.

[34] Yang, X., Hou, Y. Observed surface warming induced by urbanization in east China. Journal of Geophysical Research: Atmospheres, 2011, 116, 14113.

[35] Yang, C., Yan, F., Zhang, S. Comparison of land surface and air temperatures for quantifying summer and winter urban heat island in a snow climate city. Journal of Environmental Management, 2020, 265.

[36] Crichton, D. Role of insurance in reducing flood risk. Geneva Papers on Risk and Insurance: Issues and Practice, 2008, 33, 117–132.

[37] Tomlinson, C.J., Chapman, L., Thornes, J.E., Baker, C.J. Including the urban heat island in spatial heat health risk assessment strategies: A case study for Birmingham, UK. International Journal of Health Geographics, 2011, 10.

[38] Zhibin, R., Haifeng, Z., Xingyuan, H., Dan, Z., Xingyang, Y. Estimation of the relationship between urban vegetation configuration and land surface temperature with remote sensing. Journal of the Indian Society of Remote Sensing, 2015, 43, 89–100.

[39] Zhang, W., Zheng, C., Chen, F. Mapping heat-related health risks of elderly citizens in moun-

tainous area: A case study of Chongqing, China. Science of the Total Environment, 2019, 663, 852-866.

[40] Buscail, C., Upegui, E., Viel, J.F. Mapping heatwave health risk at the community level for public health action. International Journal of Health Geographics, 2012, 11.

[41] Tomlinson, C.J., Chapman, L., Thornes, J.E., Baker, C.J. Including the urban heat island in spatial heat health risk assessment strategies: A case study for Birmingham, UK, 2011.

[42] Ruescas, A.B., Danne, O., Fomferra, N., Brockmann, C. The land surface temperature synergistic processor in beam: A prototype towards sentinel-3. Data (Basel) 2016, 1(3), 18.

[43] Chiang, S. Mapping and tracking forest burnt areas in the Indio Maiz biological reserve using sentinel-3 SLSTR and VIIRS-DNB imagery. Sensors, 2019, 19(24), 5423

[44] Coppo, P., Ricciarelli, B., Brandani, F., Delderfield, J., Ferlet, M., Mutlow, C., …, Nieke, J. SLSTR: A high accuracy dual scan temperature radiometer for sea and land surface monitoring from space. Journal of Modern Optics, 2010, 57, 1815–1830.

[45] Wan, Z. New refinements and validation of the collection-6 MODIS land-surface temperature/ emissivity product. Remote Sensing of Environment, 2014, 140, 36–45.

[46] Sobrino, J.A., Jimenez-Mucoz, J.C., Sтria, G., Ruescas, A.B., Danne, O., Brockmann, C., …, Gottsche, F.-M. Synergistic use of MERIS and AATSR as a proxy for estimating land aurface remperature from Sentinel-3 data. Remote Sensing of Environment, 2016, 179, 149-161.

[47] Prikaziuk, E., van der Tol, C. Global sensitivity analysis of the SCOPE model in Sentinel-3 Bands: Thermal domain focus. Remote Sensing, 2019, 11(20), 2424.

[48] Remedios, J., Emsley, S. Sentinel-3 optical products and algorithm definition land surface temperature, 2012.

[49] Oke, T.R. Boundary layer climates. Boundary Layer Climates, 1987.

[50] Faisal, A., Al Kafy, A.A., Al Rakib, A., Akter, K.S., Jahir, D.M.A., Sikdar, M.S., …, Rakman, M. Assessing and predicting land use/land cover, land surface temperature and urban thermal field variance index using Landsat imagery for Dhaka Metropolitan area. Environmental Challenges, 2021, 4, 100192.

[51] Sresto, M.A., Morshed, M.M., Siddika, S., Almohamad, H., Al-Mutiry, M., Abdo, H.G. Impact of COVID-19 lockdown on vegetation indices and heat island effect: A Remote sensing study of Dhaka City, Bangladesh. Sustainability, 2022, 14(13), 7922.

[52] Keeratikasikorn, C., Bonafoni, S. Urban heat island analysis over the land use zoning plan of Bangkok by means of Landsat 8 imagery. Remote Sensing, 2018, 10, 440.

[53] Faisal, A., Al Kafy, A.A., Al Rakib, A., Akter, K.S., Jahir, D.M.A., Sikdar, M.S., ..., Rahman, M. Assessing and predicting land use/land cover, land surface temperature and urban thermal field variance index using Landsat imagery for Dhaka Metropolitan area. Environmental Challenges, 2021, 4, 100192.

[54] Ahmed, B., Kamruzzaman, M., Zhu, X., Simulating land cover changes and their impacts on land surface temperature in Dhaka, Bangladesh. Remote Sensing, 2013, 5, 5969–5998.

[55] Economidou, M., Todeschi, V., Bertoldi, P. Accelerating energy renovation investments in buildings - Financial and fiscal instruments across the EU, 2019, 174.

[56] Morabito, M., Crisci, A., Gioli, B., Gualtieri, G., Toscano, P., Di Stefano, V., …, Gensini, G.F. Urban-hazard risk analysis: Mapping of heat-related risks in the elderly in major Italian cities. PlosOne, 2015, 10, e0127277.

[57] Todeschi, V., Pappalardo, S.E., Zanetti, C., Peroni, F., De Marchi, M. Climate justice in the city: Mapping heat-related risk for climate change mitigation of the urban and peri-urban area of Padua (Italy). ISPRS International Journal of Geo-Information, 2022, 11.

[58] Wu, C., Li, J., Wang, C., Song, C., Chen, Y., Finka, M., …, Understanding the relationship between urban blue infrastructure and land surface temperature. Science of the Total Environment, 2019, 694.

[59] Yang, C., Yan, F., Zhang, S. Comparison of land surface and air temperatures for quantifying summer and winter urban heat island in a snow climate city. Journal of Environmental Management, 2020, 265, 110563.

[60] Cheval, S., Constantin, S. Black Sea impact on its west-coast land surface temperature. Theoretical and Applied Climatology, 2019, 135, 1583–1593.